Influence of Intermittent Turbulence on Air Pollution and Its Dispersion in Winter 2016/2017 over Beijing, China

Wei WEI[1], Hongsheng ZHANG[2*], Xuhui CAI[3], Yu SONG[3], Yuxuan BIAN[1], Kaitao XIAO[4], and He ZHANG[2]

1 *State Key Laboratory of Severe Weather*, *Chinese Academy of Meteorological Sciences*, *China Meteorological Administration*, *Beijing* 100081
2 *Laboratory for Climate and Ocean–Atmosphere Studies*, *Department of Atmospheric and Oceanic Sciences*, *School of Physics*, *Peking University*, *Beijing* 100871
3 *State Key Joint Laboratory of Environmental Simulation and Pollution Control*, *Department of Environmental Science*, *Peking University*, *Beijing* 100871
4 *State Key Laboratory of NBC Protection for Civilian*, *Beijing* 102205

(Received August 4, 2019; in final form November 18, 2019)

ABSTRACT

With rapid urbanization in recent years, severe air pollution has emerged as a major issue for many regions of China, especially in some metropolises. A persistent pollution case during 6 December 2016–8 January 2017 was selected to investigate the relations between turbulent intermittency and frequent $PM_{2.5}$ (particulate matters with diameter less than 2.5 μm) pollution events over the metropolitan region of Beijing, China. The accumulation of $PM_{2.5}$ near the surface frequently occurred as a combined result of strong inversion layers, stagnant winds, high ambient humidity levels, and stable stratification during this case. Arbitrary-order Hilbert spectral analysis indicated that steep decreases in the $PM_{2.5}$ concentration were simultaneous with the occurrence of intermittent turbulence and strong vertical mixing. A wind profiler observation revealed existence of low-level jets (LLJs) at the end of the polluted periods, suggesting that the upper-level turbulent mixing accompanied by the wind shear of LLJ was transported downward and enhanced the vertical mixing near the surface, which might have caused an abrupt reduction in $PM_{2.5}$ and improvement in air conditions.

Key words: intermittent turbulence, $PM_{2.5}$, stable stratification, Beijing

Citation: Wei, W., H. S. Zhang, X. H. Cai, et al., 2020: Influence of intermittent turbulence on air pollution and its dispersion in winter 2016/2017 over Beijing, China. *J. Meteor. Res.*, **34**(1), 176–188, doi: 10.1007/s13351-020-9128-4.

1. Introduction

Due to rapid urbanization in recent years, air pollution issues are prevalent in most parts of China. The air quality problem in Beijing is receiving an increasing amount of attention. Considering its adverse impacts on human health (Nel, 2005; Dominici et al., 2014; Thompson et al., 2014; Zheng S. et al., 2015), $PM_{2.5}$ (particulate matters with diameter less than 2.5 μm) pollution has become severe (Hu et al., 2014; Wang H. et al., 2014; Wang L. L. et al., 2014), as a combined result of the consumption of fossil fuel, the production of secondary pollutants, regional transport, synoptic weather conditions, and boundary-layer feedback (Wang et al., 2010; Zheng G. J. et al., 2015; Petäjä et al., 2016; Ye et al., 2016; Zhang et al., 2016).

Occurring in the atmospheric boundary layer (ABL), the evolution of air pollution is associated with characteristics of the ABL (Bressi et al., 2013; Gao et al., 2016; Tang et al., 2016; Ye et al., 2016). A series of previous studies have addressed the effects of dynamic mechanisms on air pollution on different atmospheric scales including climate change (Dawson et al., 2007), large-scale meteorological conditions (Wang L. L. et al., 2014; Jia et al., 2015; Ye et al., 2016), regional transport (Wang L. L. et al., 2014; Miao et al., 2017), and atmospheric stability (Zhang et al., 2012; Ye et al., 2016; Miao et al., 2017; Yin and Wang, 2017). In contrast, the studies aiming at

Supported by the National Key Research and Development Program of China (2016YFC0203300) and National Natural Science Foundation of China (91544216 and 41705003).

*Corresponding author: hsdq@pku.edu.cn.

the effects of intermittent turbulence on the particle transport is limited. Turbulent behavior has a key role in the transport, accumulation, and dispersion of atmospheric pollutants (Rodriguez et al., 1995; Schäfer et al., 2006; Walters et al., 2007; Ren et al., 2018), and the turbulence in the stable boundary layer (SBL) is weak and intermittent at a variety of heights, temporal scales, and spatial locations (Klipp and Mahrt, 2004; Salmond, 2005; Mahrt, 2014). As the intermittent fluxes were determined to be responsible for a large fraction of the turbulent exchange between the surface and the upper boundary layer (Acevedo and Fitzjarrald, 2003; Yagüe et al., 2006; Vindel and Yagüe, 2011; Helgason and Pomeroy, 2012; Noone et al., 2013), the intermittent turbulence is expected to have an important role in the diffusion and transport of air pollutants within the ABL (Shen et al., 2017).

Analytical techniques have a significant impact on analyses of intermittent turbulence. Traditional methods (such as Fourier analysis and wavelet analysis) have some disadvantages when they are applied to the study of turbulent flows. A Fourier analysis requires a linear system and a stationary dataset. A wavelet analysis is basically an adjustable window Fourier spectral analysis and is not appropriate for nonlinear systems considering the intrawave frequency modulation (Huang et al., 1998). The non-stationarity and nonlinearity of intermittent turbulence limit the methods that analyses can support. Recently, a new technique that is referred to as arbitrary-order Hilbert spectral analysis (Huang et al., 2011) has been developed and has shown its advantages and validity in the application of turbulent flows and intermittency (Wei et al., 2016, 2017, 2019).

Some studies (Strassburger and Kuttler, 1998; Baumbach and Vogt, 1999; Kalthoff et al., 2000; Reitebuch et al., 2000; Seibert et al., 2000; Salmond, 2005; Salmond and McKendry, 2005; Hu et al., 2013) have investigated the relation between intermittent turbulence and air quality and identified the positive contribution of intermittent turbulence to the increasing ozone concentration during nighttime near the surface. Some perspectives note that the instability of the turbulence in the SBL is helpful in reducing particle materials (Grange et al., 2013). Few studies specify the role of nocturnal intermittent turbulence in air pollution, especially in severe $PM_{2.5}$ events. As indicated by Miao et al. (2017), the nocturnal ABL can significantly affect air pollution by intermittent turbulence; however, the intermittent turbulence and its interaction with other mesoscale motions in the ABL hinder the study of pollutants dispersion in the nocturnal ABL, particularly in regions of complex terrain such as Beijing (Zhang et al., 2016; Miao et al., 2017). For the Beijing region, air pollution shows its uniqueness and severity in terms of duration and pollutant concentration (Chen and Wang, 2015; Zheng G. J. et al., 2015; Cai et al., 2017; Cheng et al., 2017), and $PM_{2.5}$ pollution is an outstanding issue compared with other kinds of pollutants (Hu et al., 2014; Zhang et al., 2016).

Based on these considerations, we focus on the influence of turbulent intermittency on the vertical dispersion of $PM_{2.5}$ over the Beijing region in winter. To achieve this goal, the intermittent turbulence is measured in this study by using a self-adaptive method named arbitrary-order Hilbert spectral analysis (Huang et al., 2011), and the relevance of intermittent turbulence to the $PM_{2.5}$ is identified. Then, the dispersion of $PM_{2.5}$ and ozone is analyzed to verify the conclusion although the concentration of ozone in winter is considerably less than the air pollution criteria. In Section 2, we introduce the data and method used in this study. The evolution of pollution events and the role of intermittent turbulence in these events are discussed in Section 3. Section 4 summarizes our conclusions.

2. Observation and method

2.1 *Observation and data*

In 2016/2017 winter, severe air pollution accompanied by high $PM_{2.5}$ concentrations occurred in the Beijing region. Figure 1 presents a typical comparison between a polluted day and a clean day in the morning (0070–0900 LST, local standard time). In this study, a 34-day period from 6 December 2016 to 8 January 2017 was selected to investigate the effects of intermittent turbulence on air pollution. During this period, three pollution alerts were issued by the Beijing authorities due to the extremely high $PM_{2.5}$ concentration, and 21 of these 34 days attained an hourly averaged $PM_{2.5}$ concentration greater than 200 μg m^{-3}. The shaded areas in Fig. 2a denote the dates on which the hourly averaged $PM_{2.5}$ concentration was greater than 200 μg m^{-3}. Specifically, the first 5-day pollution alert from 17 to 21 December 2016 attained the first-ever "red alert," the second episode from 24 to 25 December 2016 was given "blue alert," and the third episode from 30 December 2016 to 9 January 2017 was "orange alert," where the red/blue/orange alerts are categorized by predicted seriousness and duration of air pollution events (Cheng et al., 2017). For convenience, six polluted periods with high $PM_{2.5}$ concentration are named Case-1, 2, 3, 4, 5, and 6 (refer to the shaded areas in Fig. 2). Twenty-one polluted days (6 periods) had a $PM_{2.5}$ concentration that exceeded 200 μg m^{-3}, which

Fig. 1. Comparison between a polluted day (left, 21 December 2016) and a clean day (right, 23 December 2016). Photos were taken near the Beijing TV station in the morning between 0700 and 0900 LST.

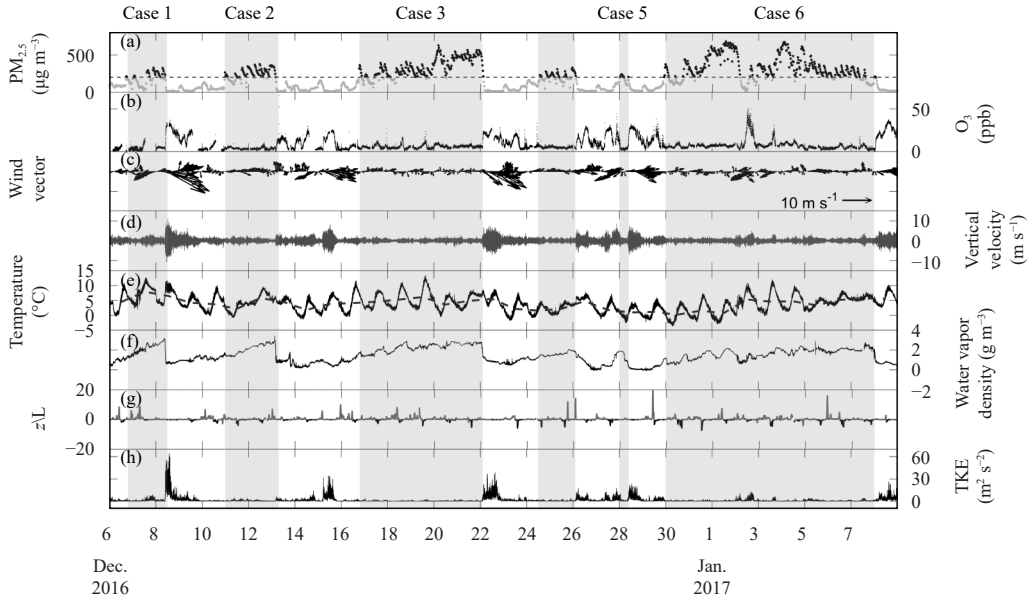

Fig. 2. Temporal distributions of (a) $PM_{2.5}$ concentration (30 min), (b) ozone concentration (1 min), (c) wind vector (30 min), (d) vertical velocity (10 Hz), (e) temperature (10 Hz, dashed line refers to daily average temperature), (f) density of water vapor (10 Hz), (g) stability parameter z/L (1 min), and (h) TKE (1 min) from 6 December 2016 to 8 January 2017. Shaded areas refer to polluted periods and remaining areas correspond to clean periods.

were 7–8, 11–12, 17–21, 24–25, 28, 30–31 December 2016, and 1–7 January 2017. The remaining days were identified as clean days.

The measurements of the $PM_{2.5}$ and turbulence were collected in Beijing (39°59′N, 116°18′E). The instruments (Table 1) were situated at a height of 2.6 m on the top of a building of the School of Physics, Peking University, which extended to 25 m above the surface. The $PM_{2.5}$ data were collected by using a Thermo-Fisher Sci. Co. Series FH-62-C14 and transformed into 30-min aver-

Table 1. Particulars of the instruments used in this study

Type		Manufacturer	Technical parameter
Continuous ambient fine particle monitor	FH-62-C14	Thermo-Fisher Sci. Co., USA	$PM_{2.5}$ range: 0–5000 μg m^{-3}; Precision: 2 μg m^{-3}
Integrated CO_2/H_2O Open-Path Gas Analyzer and 3D Sonic Anemometer	IRGASON	CAMPBELL Co., USA	Wind speed range: ± 65.553 m s^{-1}; Precision: 1 mm s^{-1} (u_x/u_y), 0.5 mm s^{-1} (u_z); Accuracy: < ± 8 cm s^{-1} (u_x/u_y), < 4 cm s^{-1} (u_z) Temperature range: −5 to 60°C; Precision: 0.025°C; Accuracy: ± 0.15°C (0–50°C) H_2O range: 0–42 g m^{-3}; Precision: 0.0035 g m^{-3}

aged series to remove outliers. The variation of the $PM_{2.5}$ concentration is shown in Fig. 2a. Wind, temperature, and water vapor fluctuations were logged at 10 Hz by using an IRGASON Integrated CO_2/H_2O Open-Path Gas Analyzer and 3D Sonic Anemometer (CAMPBELL Co., USA) to analyze the intermittent turbulence, through derivation of the turbulent kinetic energy (TKE) $\bar{e} = (\overline{u'^2} + \overline{v'^2} + \overline{w'^2})/2$ and the stability parameter $z/\mathrm{L} = -\kappa z \mathrm{g}\overline{w'\theta'}/\bar{\theta}u_*^3$, in which the overline represents the time average; e is the TKE; u', v', *and* w' denote the longitude, lateral, and vertical fluctuations of the wind vector, respectively; θ' is the temperature fluctuation; u_* is friction velocity in the form $u_* = (\overline{u'w'}^2 + \overline{v'w'}^2)^{1/4}$; z is the observation height; g is the gravitational acceleration; L is the Obukhov length, and $\kappa = 0.4$ is the von Karman constant, based on an averaging time of 1 min.

Strict quality control was conducted on the data used in this study, including detrending (block average), error flagging, spike detection, and coordinate rotation (double rotation). The observation by an L-band radiosonde radar mounted in southern Beijing was adopted to illustrate the vertical structure of the ABL. During the case period, L-band radiosonde radar was implemented twice a day at 0800 and 2000 LST. The characteristics of the wind field were obtained by using a CFL-16 wind profiler, which captured the 25 levels of wind speed and direction below about 3 km with a vertical resolution of 120 m. For details about the performance of the CFL-16 wind profiler, refer to Table 1 in Miao et al. (2018).

2.2 *Method*

The flow in the ABL is highly non-linear and non-stationary and the intermittency in stable conditions complicates the analysis. To quantify the level of turbulent intermittency in the SBL, a recently proposed method named arbitrary-order Hilbert spectral analysis (HSA; Huang et al., 2008) was applied to the vertical velocity in this study. The arbitrary-order HSA is developed from the Hilbert–Huang transform (Huang et al., 1998, 1999), which is local in both the physical domain and the frequency domain, and is data-adaptive without priori assumptions. Thus, the HSA is more favorable for the investigation of intermittent turbulence compared with traditional methods (e.g., Fourier analysis or wavelet transform).

The first step is the empirical mode decomposition, which separates a time series $X(t)$ into a group of intrinsic mode functions $C_i(t)$ and a residual $r_n(t)$, where $X(t)$ refers to the vertical velocity with a length of 30 min. The decomposition process is described as follows (Huang et al., 1998, 1999):

1) The upper envelope $e_{\max}(t)$ is constructed from the local maxima of $X(t)$ by using the cubic spline interpolation. The lower envelope $e_{\min}(t)$ can be formed likewise.

2) The mean is defined as $m_1(t) = [e_{\max}(t) + e_{\min}(t)]/2$, which produces the first local detail $h_1(t) = X(t) - m_1(t)$.

3) The variable $h_1(t)$ is the first intrinsic mode function $C_1(t) = h_1(t)$, if (i) the difference between the number of local extrema and the number of zero-crossings is zero or one, and (ii) the running mean values of $e_{\max}(t)$ and $e_{\min}(t)$ are zero. The function is subtracted from $X(t)$ to obtain the first residual $r_1(t) = X(t) - C_1(t)$, which is regarded as the new signal in the first step. If the two criteria are not satisfied, $h_1(t)$ is considered as a new time series to form the lower and upper envelopes and the mean $m_{11}(t)$. Subtracting $m_{11}(t)$ from $h_1(t)$ creates a new local detail $h_{11}(t)$, which is re-evaluated to determine if it satisfies both criteria. If $h_{11}(t)$ does not, this process is repeated k times until $h_{1k}(t)$ is an intrinsic mode function $C_1(t) = h_{1k}(t)$.

Repeat the above 1)–3) until the residual $r_n(t)$ becomes a monotonic function. The standard deviation criterion (Huang et al., 1998) is used to avoid over-sifting the intrinsic mode functions. $X(t)$ can be expressed as $X(t) = \sum_{i=1}^{n} C_i(t) + r_n(t)$. The Hilbert transform (Cohen, 1995) can be applied to each mode $C_i(t)$ to obtain the analytical signal $C_i^A(t) = C_i(t) + j\tilde{C}_i(t) = A_i(t)\exp[j\,\theta_i(t)]$, where $\tilde{C}_i(t)$ is defined as $\tilde{C}_i(t) = \frac{1}{\pi}\int_{-\infty}^{\infty} \frac{C_i(\tau)}{t-\tau}\mathrm{d}\tau \frac{\mathrm{d}\theta_i}{\mathrm{d}t}$, $A_i(t)$ is

the instantaneous amplitude and $\theta_i(t)$ is the instantaneous phase. Further, the instantaneous frequency can be defined as $\omega_i(t) = \frac{1}{2\pi}\frac{\mathrm{d}\theta_i}{\mathrm{d}t}$.

With the time series of $\omega_i(t)$ and $A_i(t)$, the Hilbert spectrum, $H(\omega,t)$, is expressed as a frequency–time distribution of the amplitude. Using the joint probability density function [PDF; $p(\omega,A)$], $H(\omega,t)$ can be further expressed as $h(\omega) = \int p(\omega,A)A^2\mathrm{d}A$. The arbitrary-order Hilbert spectrum is defined as $\mathcal{L}_q(\omega) = \int p(\omega,A)A^q\mathrm{d}A$, where $q \geqslant 0$ is the arbitrary moment.

In the case of scale invariance, $\mathcal{L}_q(\omega) \approx \omega^{-\xi(q)}$, in which $q \geqslant 0$ is the order, ω is the frequency, and $\xi(q)$ is the scaling exponent function. In the case of fully developed turbulence, the scaling exponent function $\xi(q)$ and order q should follow $\xi(q) - 1 = q/3$ (Kolmogorov, 1941). Moreover, the larger that $\xi(q) - 1$ deviates from $q/3$, the stronger the intermittent turbulence. In Section 3.2, the scaling exponent function will be used to identify the characteristics of intermittent turbulence.

3. Results

3.1 *Overview of meteorological conditions*

Figure 2 illustrates the fluctuation distributions of $PM_{2.5}$, ozone, wind, temperature, water vapor density, stability parameter, and TKE. Compared with the distribution of $PM_{2.5}$ in Fig. 2a, the most notable feature in Fig. 2b is that the concentration of ozone near the surface exhibits an opposite change to that of $PM_{2.5}$. The concentration of ozone increases at the same moment of the sharp drop in $PM_{2.5}$. Other studies (Shao et al., 2018) that focused on this pollution event in Beijing also revealed the opposite distribution between $PM_{2.5}$ and ozone (refer to their Fig. 2). The following analyses reveal that the same mechanism underlies the evolution of $PM_{2.5}$ and the ozone concentration near the surface. The wind speed during polluted periods (shaded areas in Fig. 2c) is weak. The dissipation of air pollutants is generally related to stronger northwesterly wind, which is consistent with previous studies (Shao et al., 2018). For comparison, Table 2 provides the statistical results of different variables. The values of the polluted and clean periods are calculated by using observations from all six polluted cases (shaded areas in Fig. 2) and the same goes for values of clean periods (unshaded areas in Fig. 2). For the magnitude of vertical velocity (Fig. 2d), the maximum for the clean periods is much greater with a value of 10.95 m s^{-1}, whereas the vertical velocity during the polluted periods is generally less than 5.0 m s^{-1}, which implies weak turbulence motions. The diurnal variation also presents weaker vertical fluctuations during polluted days (Fig. 3c) than those on clean days (Fig. 3d).

In terms of temperature (Fig. 2e), despite the diurnal variation, the daily average temperature shows agreement with the change in the $PM_{2.5}$ concentration. For six polluted cases, the daily mean temperature (dashed line in Fig. 2e) during the polluted periods are higher than those of the clean periods, and the temperature values of the clean periods generally correspond to the valleys. The diurnal variation in Figs. 3e–f further confirms a warmer boundary layer during the polluted periods. According to the direct aerosol effect (Charlson et al., 1992), the scattering of solar radiation by the particles in the atmosphere reduces the incoming energy and cools the surface, and the radiative absorption by absorbing aerosol compounds heats the upper atmosphere and increases the air temperature. Therefore, the chemical composition has an important role in the evolution of temperature during heavily polluted events. Shao et al. (2018) thoroughly reviewed the chemical composition and sources of this pollution event during the 2016/2017 winter in Beijing and noted that carbonaceous aerosol [organic carbon (OC) and element carbon (EC)] and SO_4^{2-}, NO^{3-}, and NH^{4+} [secondary inorganic aerosol (SIA) species] were two major parts (refer to their Fig. 3b for the results of $PM_{2.5}$). Although high-polluted industries have been closed or shifted and coal consumption has been restricted in Beijing since 2013 due to the Clean Air Action Plan by the Beijing municipal government, regional circulation can also transport pollutants from neighboring provinces (such as Shanxi, Hebei, and Shandong provinces with large amounts of population and energy-intensive industries) into the Beijing region and cause heavily polluted events (Yin and Wang, 2017; Zhong et

Table 2. Statistical results [mean ± standard deviation (SD); maxima (Max)] in polluted and clean periods

Variable		$PM_{2.5}$ (μg m^{-3})	Temperature (°C)	Water vapor density (g m^{-3})	Magnitude of W (m s^{-1})	z/L at night	TKE (m^2 s^{-2})
Polluted	Mean ± SD	244 ± 158	4.2 ± 3.0	1.68 ± 0.98	0.27 ± 0.30	−0.29 ± 1.29	1.26 ± 3.26
	Max	678	13.4	3.43	5.00	12.24	12.59
Clean	Mean ± SD	107 ± 57	3.1 ± 2.6	0.97 ± 0.68	0.42 ± 0.44	−0.18 ± 0.67	2.14 ± 3.23
	Max	199	11.6	2.79	10.95	1.47	64.84

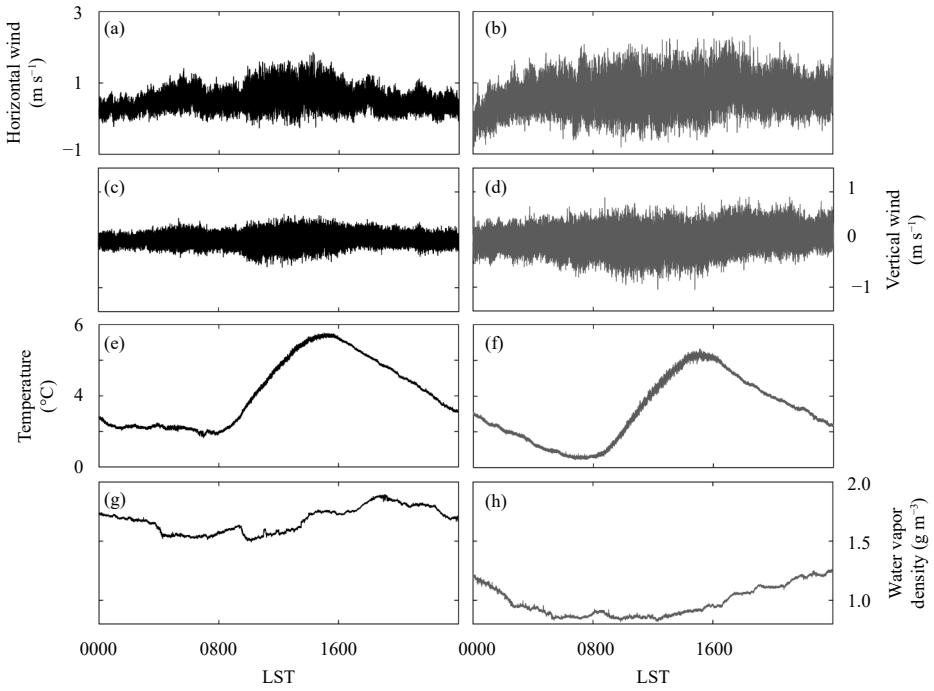

Fig. 3. Comparison between the polluted periods (left panels) and the clean periods (right panels) of the diurnal change (10 Hz): (a, b) horizontal wind speed, (c, d) vertical velocity, (e, f) temperature, and (g, h) density of water vapor.

al., 2017). In the case of heavily polluted events such as those in Beijing, Petäjä et al. (2016) revealed a positive feedback between the aerosol concentration and the boundary layer characteristics: the high concentration of pollutants in the boundary layer reduces the surface temperature and heats the upper layers, which produces a stronger inversion layer with weakened turbulence and a lower boundary layer height. The low boundary layer height further increases the pollutant concentration. Figure 4a shows the vertical structure of temperature at heights less than 1500 m, where strong inversion layers are observed during the heavily polluted periods (denoted by dashed boxes). The deepened inversion layer near the surface is caused by the interaction between the pollutants and the boundary layer characteristics.

The atmospheric humidity is closely related to $PM_{2.5}$

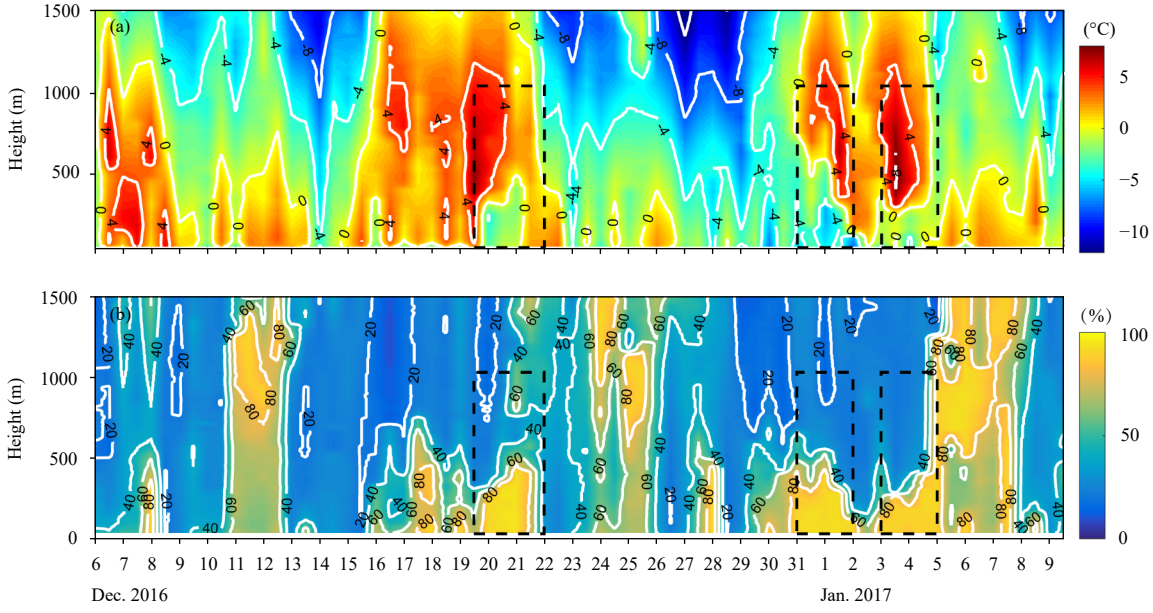

Fig. 4. Height–time cross-sections of (a) temperature and (b) RH. Dashed boxes denote the inversion layers and explosive growth in RH.

concentration. The water vapor density (Fig. 2f) steadily increases during each polluted period and abruptly decreases to below 0.5 g m^{-3}, accompanied by a sharp drop in $PM_{2.5}$ concentration. The water vapor density (Figs. 3g, h) for polluted periods is notably higher during the whole day. Similar to that of temperature, the vertical structure of relative humidity (RH) in Fig. 4b presents quick deepening processes during the heavily polluted periods. The values of RH below 500 m are in general higher than 80% and the maximal RH can reach 95%.

Based on analyses of the meteorological variables, unfavorable diffusion conditions, local emissions, and regional transport from other areas are responsible for the severe air pollution in the Beijing region. In this study, the stagnant wind and high humidity aggravate the levels of air pollution. The persistence of weak wind during the polluted periods inhibits the transport of pollutants and causes accumulation, whereas the strong wind speed at the beginning of the clean periods contributes to the diffusion of pollutants and the abrupt decrease in the $PM_{2.5}$ concentration. The water vapor density continuously increases during each polluted period. In the late period of pollution with high ambient humidity, heterogeneous aqueous reactions accelerate the formation of secondary inorganic aerosols, leading to rapid increase of the $PM_{2.5}$ concentration (Hu et al., 2008; Wang et al., 2012; Quan et al., 2014, 2015).

With rising ambient humidity, the secondary formation of sulfates, nitrates, and ammonium (SNA) presents an exponential, logarithmic, or linear increase, including the droplet-mode SNA concentration, the ratio of droplet-mode SNA to the total SNA, the fraction of SNA in droplet-mode particles, and the mass median aerodynamic diameter of SNA. The polluted periods are generally characterized by a stronger inversion layer, higher humidity, weak wind, and low-pressure systems (Wang L. L. et al., 2014; Zhong et al., 2017).

Due to the prevailing continental monsoon climate and local topography in Beijing, an inversion layer frequently develops near the surface almost every night and during the daytime in winter, which produces stable stratification and weak turbulence transport (Tao et al., 2007). Under the influence of such a continental monsoon climate, large diurnal difference in temperature in winter favors the formation of a statically stable boundary layer over the Beijing region. Surrounded by mountains to the north, northwest, and west, Beijing experiences the radiative cooling of the ground surface and mountain–valley circulation, which may have caused frequent occurrence of inversion in winter (Xia, 2006).

Figure 2g delineates the stability condition during this case, with z/L much larger than 1 on polluted nights. The mean value of z/L on polluted nights is 0.29 while that for clean nights is only 0.18, which confirms the more stable stratification during the polluted period. The distribution of TKE in Fig. 2h further verifies the results of stability and turbulence strength, where the TKE is weak during the polluted periods but suddenly increases. Figure 5 compares the typical surface weather conditions between the polluted condition (consider 0200 LST 21 December 2016 as an example) and the clean condition (1400 LST 22 December 2016). In general, the heavy pollution event is accompanied by a low pressure system that dominates this region (left panel in Fig. 5). Under the influence of the southeast-moving anticyclone system, the isobars become dense and the surface wind speed strengthens, which provides an ideal condition for the dissipation of air pollutants (right panel in Fig. 5).

3.2 *Mechanism of $PM_{2.5}$ dispersion*

To discuss the mechanism that underlies the dispersion of $PM_{2.5}$, two cases (the "red alert" Case 3 and the "orange alert" Case 6) are analyzed in detail, which are characterized by high $PM_{2.5}$ concentration and long duration. Figure 6 highlights the characteristics of $PM_{2.5}$ and ozone for these two cases, in which red boxes specify the opposite changes between $PM_{2.5}$ and ozone. Three abrupt dips of $PM_{2.5}$ simultaneously occur with a sharp rise in ozone (see the boxes). The same mechanism is assumed to underlie the evolution of both $PM_{2.5}$ and ozone.

Some previous studies have focused on the surface ozone pollution (Strassburger and Kuttler, 1998; Baumbach and Vogt, 1999; Kalthoff et al., 2000; Reitebuch et al., 2000; Seibert et al., 2000; Salmond, 2005; Salmond and McKendry, 2005; Hu et al., 2013). These studies demonstrate that ozone is formed as a result of the photodissociation of nitrogen dioxide in the presence of ultraviolet light, and the concentration of ozone near the surface is expected to decrease with time in the SBL and present diurnal changes (Wang et al., 2008; Tang et al., 2009; Ding et al., 2013). However, in the presence of intermittent "bursts" of turbulence, trapped ozone in the residual layer above may be the source of low-level pollution. Intermittent turbulence and vertical mixing in the SBL can transport ozone that is stored in the residual layer down to the surface and produce an increasing ozone concentration near the surface. By referring to the formation and dispersion of ozone, $PM_{2.5}$ pollution is nearly opposite to ozone. Due to the local vehicle exhaust of heavy traffic, energy consumption for indoor heating and industrial production, and low-level regional transport

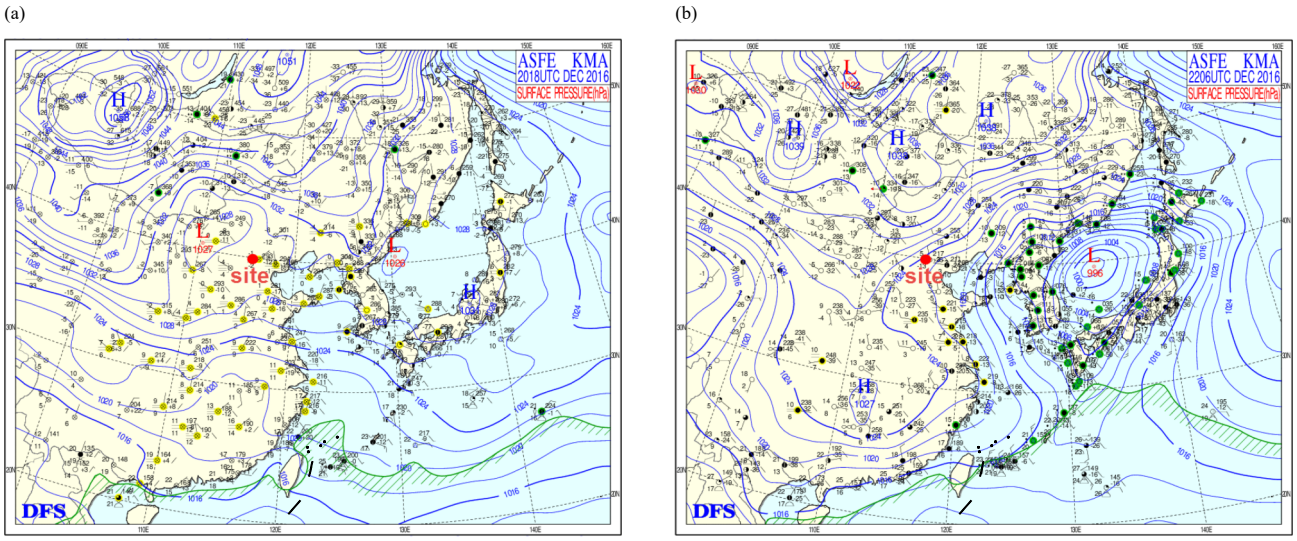

Fig. 5. Comparison of typical surface weather conditions at (a) 0200 LST 21 and 1400 LST 22 December 2016. Red dots refer to Beijing. Weather charts were obtained from the Korea Meteorological Administration (https://web.kma.go.kr/eng/weather/images/analysischart.jsp).

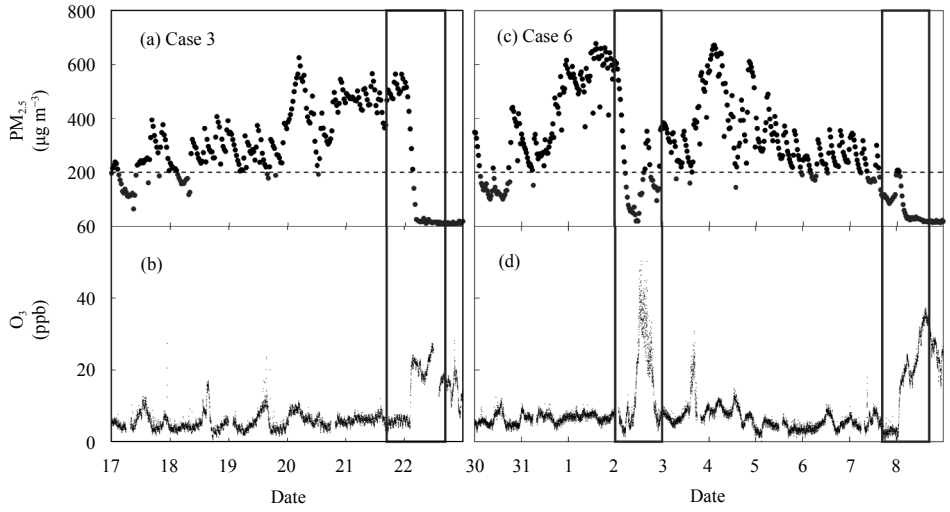

Fig. 6. Distributions of $PM_{2.5}$ and ozone concentrations in (a, b) Case 3 and (c, d) Case 6 (boxes denote the abrupt change in pollutants).

contribution (Yu et al., 2013; Wang et al., 2015), a substantial amount of $PM_{2.5}$ is formed and transported at lower levels. In this case, the vertical turbulent flux can transport low-level pollutants upward and alleviate the $PM_{2.5}$ pollution near the surface.

Although the structure and mechanisms of the SBL (especially in very stable conditions) are less understood (Mahrt, 1998), some studies suggest that turbulence in very stable conditions is weak, patchy, and intermittent (Mahrt, 2014; Wei et al., 2016). Considering that intermittent fluxes are responsible for a large fraction of the turbulent exchange between the surface and the upper boundary layer and the effect of intermittent turbulence on ozone pollution has been verified (Poulos et al., 2002; Salmond, 2005), it is necessary to investigate the behavior of turbulence near the surface. The arbitrary-order HSA (Huang et al., 1998) is employed to quantify the intermittent turbulence. As mentioned in Section 2.2, any distinction from the theoretical value $q/3$ suggests the impact of intermittency. Considering the inaccuracy of the estimation of higher-order moments caused by the finite signal length (Frisch, 1995), we set order $q \leqslant 4$. Figures 7a and 7b illustrate the behavior of $\xi(q)-1$ compared with $q/3$, where orders $q \leqslant 4$. The results show a set of convex curves of scaling exponent functions for both cases while the convexity and/or distinction from $q/3$ is much stronger during the dispersion periods (blue dotted lines in Figs. 7a, b), which reveals that the turbu-

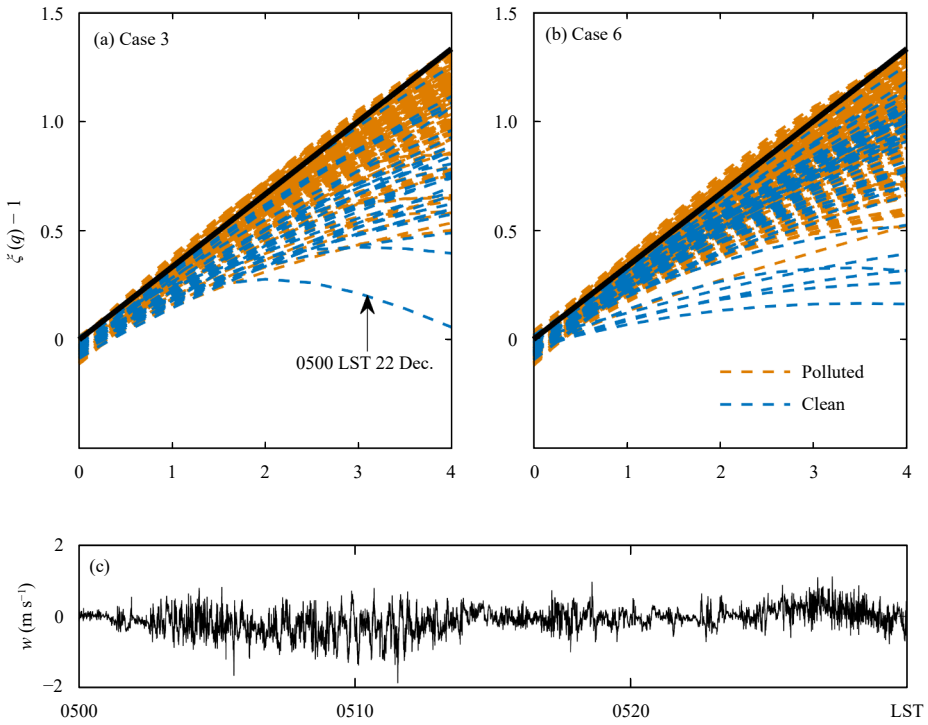

Fig. 7. Representation of the Hilbert-based scaling exponent function $\xi(q)-1$ of (a) Case 3 and (b) Case 6 compared with $q/3$ (black straight lines). (c) The original vertical velocity during 0500–0530 LST 22 December 2016.

lence during the dispersion periods is intermittent. The largest distinction from $q/3$ is denoted by the arrow in Fig. 7a, while Fig. 7c shows the original vertical velocity during 0500–0530 LST 22 December 2016. This time series provides an irregularly alternate occurrence of strong "bursts" and weak turbulence, which verifies the intermittent turbulence.

Intermittent turbulence in the SBL can be attributed to different reasons, including gravity waves (Sorbjan and Czerwinska, 2013), solitary waves (Terradellas et al., 2005), and low-level jets (LLJs; Mahrt, 2014; Banta et al., 2006, 2007). According to the statistical results in Table 2, the kinetic and thermodynamic results confirm strongly stabilized conditions during the accumulation periods of air pollution, compared with strong wind and weak stability at the end of the polluted periods. To detect the possible reason for turbulence at the end of the polluted periods, the wind field obtained from the CFL-16 wind profiler is carefully checked. The wind profile results show that the strong wind at the end of the polluted periods is generally associated with the occurrence of LLJs. Figure 8 shows three profiles to illustrate the occurrence of LLJs (dashed line profile for Case 3; dash-dotted and solid line profiles for Case 6). Previous studies (Banta et al., 2006; Karipot et al., 2008; Deb Burman et al., 2018) have shown that LLJs can serve as an important source of turbulence in the SBL. The profile of the LLJs reveals strong wind shear aloft, which causes turbulent mixing at upper levels. The turbulence is transported downward and enhances turbulent mixing near the surface. Different from the continuous turbulence by the surface shear, the LLJ-associated turbulence is intermittent.

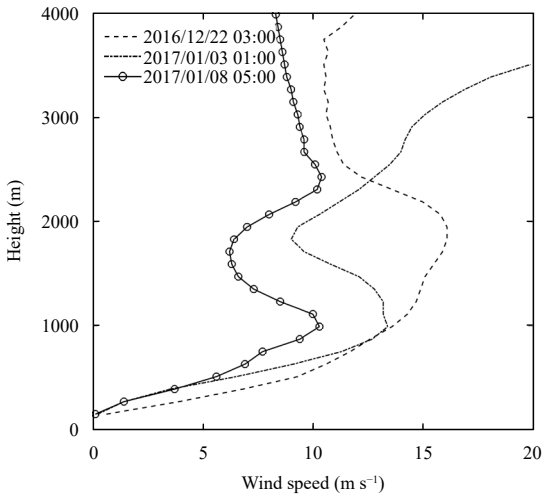

Fig. 8. Sample LLJ profiles of two cases (dashed line for Case 3; dash-dotted and solid lines for Case 6).

We summarize the effect of intermittent turbulence on the dispersion of low-level pollutants in Fig. 9. In the

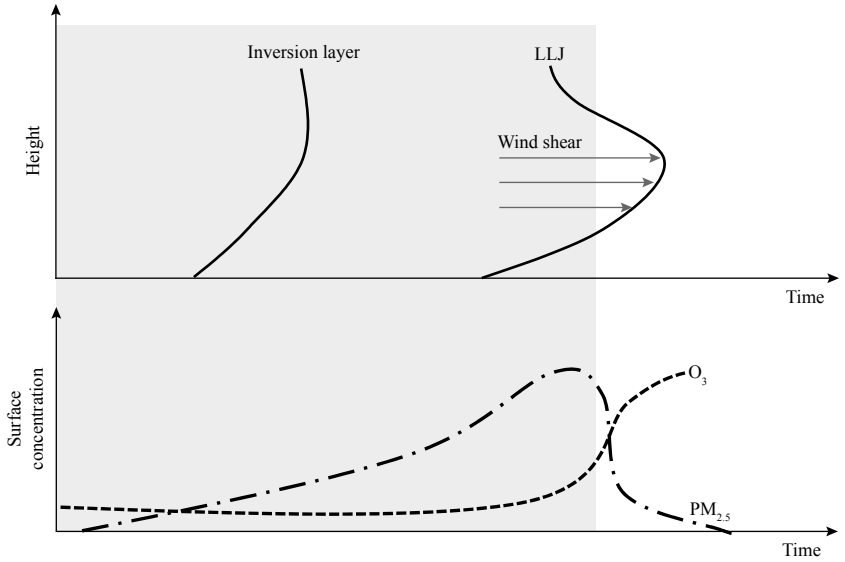

Fig. 9. Schematic of the effect of intermittent turbulence on $PM_{2.5}$ dispersion (shaded areas refer to the periods of accumulation).

first stage (shaded areas), due to favorable meteorological conditions (e.g., weak wind and strong inversion layer), $PM_{2.5}$ accumulates near the surface and the concentration of pollutants gradually increases. In the existence of LLJs, the aloft wind shear provides an uplift source of turbulence. The upper-level turbulence then transports downward and intermittently enhances the turbulent mixing near the surface. The intermittent turbulent mixing positively contributes to the vertical transport of $PM_{2.5}$, which improves the air quality near the surface. In addition, the behavior of $PM_{2.5}$ is opposite to that of ozone in previous studies (Kalthoff et al., 2000; Salmond and McKendry, 2005), which demonstrates that intermittent turbulence in the SBL transports aloft ozone to the lower levels and causes an increasing ozone concentration at lower levels.

4. Summary

A persistent and highly influential $PM_{2.5}$ air pollution event from 6 December 2016 to 8 January 2017 over the Beijing region was selected to investigate the role of intermittent turbulence on the transport of air pollutants. To quantify the turbulent intermittency, the arbitrary-order Hilbert spectral analysis is applied to this study.

In addition to the local emissions, the meteorological conditions are crucial to the accumulation, transport, and diffusion of $PM_{2.5}$. Due to the prevailing continental monsoon climate and topography in the vicinity of Beijing, stable stratification frequently occurs during winter, which provides favorable meteorological conditions for the local storage of air pollutants. The severe pollution events are characterized by a stronger inversion layer, stagnant winds, and higher ambient humidity levels. The persistent weak wind accompanied by the low pressure system implies weak turbulent transport near the surface, and the high density of water vapor accelerates the formation of secondary inorganic aerosol, which causes a rapid increase in $PM_{2.5}$. The concentration of ozone presents a completely different behavior than that of $PM_{2.5}$.

The arbitrary-order Hilbert spectral analysis reveals that the turbulence at the end of polluted periods is intermittent. From observation of the CFL-16 wind profiler, LLJs were detected immediately before the dispersion of $PM_{2.5}$. The LLJ-associated wind shear is an important source of intermittent turbulence in the SBL. The intermittently enhanced turbulent mixing near the surface transports $PM_{2.5}$ upward and improves the air quality.

Acknowledgments. Photos in Fig. 1 are authorized by Mr. Zou Yi, who promoted BeijingAirNow at http://weibo.com/p/1005051000481815.

REFERENCES

Acevedo, O. C., and D. R. Fitzjarrald, 2003: In the core of the night-effects of intermittent mixing on a horizontally heterogeneous surface. *Bound.-Layer Meteor.*, **106**, 1–33, doi: 10.1023/a:1020824109575.

Banta, R. M., Y. L. Pichugina, and W. A. Brewer, 2006: Turbulent velocity-variance profiles in the stable boundary layer generated by a nocturnal low-level jet. *J. Atmos. Sci.*, **63**, 2700–2719, doi: 10.1175/jas3776.1.

Banta, R. M., L. Mahrt, D. Vickers, et al., 2007: The very stable boundary layer on nights with weak low-level jets. *J. Atmos. Sci.*, **64**, 3068–3090, doi: 10.1175/jas4002.1.

Baumbach, G., and U. Vogt, 1999: Experimental determination of the effect of mountain-valley breeze circulation on air pollution in the vicinity of Freiburg. *Atmos. Environ.*, **33**, 4019–4027, doi: 10.1016/s1352-2310(99)00143-0.

Bressi, M., J. Sciare, V. Ghersi, et al., 2013: A one-year comprehensive chemical characterisation of fine aerosol ($PM_{2.5}$) at urban, suburban and rural background sites in the region of Paris (France). *Atmos. Chem. Phys.*, **13**, 7825–7844, doi: 10.5194/acp-13-7825-2013.

Cai, W. J., K. Li, H. Liao, et al., 2017: Weather conditions conducive to Beijing severe haze more frequent under climate change. *Nat. Climate Change*, **7**, 257–262, doi: 10.1038/nclimate3249.

Charlson, R. J., S. E. Schwartz, J. M. Hales, et al., 1992: Climate forcing by anthropogenic aerosols. *Science*, **255**, 423–430, doi: 10.1126/science.255.5043.423.

Chen, H. P., and H. J. Wang, 2015: Haze days in North China and the associated atmospheric circulations based on daily visibility data from 1960 to 2012. *J. Geophys. Res. Atmos.*, **120**, 5895–5909, doi: 10.1002/2015jd023225.

Cheng, N. L., D. W. Zhang, Y. T. Li, et al., 2017: Spatio-temporal variations of $PM_{2.5}$ concentrations and the evaluation of emission reduction measures during two red air pollution alerts in Beijing. *Sci. Rep.*, **7**, 8220, doi: 10.1038/s41598-017-08895-x.

Cohen, L., 1995: *Time-Frequency Analysis*. Prentice Hall, Englewood Cliffs, NJ, 153–161.

Dawson, J. P., P. J. Adams, and S. N. Pandis, 2007: Sensitivity of $PM_{2.5}$ to climate in the eastern US: A modeling case study. *Atmos. Chem. Phys.*, **7**, 4295–4309, doi: 10.5194/acp-7-4295-2007.

Deb Burman, P. K., T. V. Prabha, R. Morrison, et al., 2018: A case study of turbulence in the nocturnal boundary layer during the Indian summer monsoon. *Bound.-Layer Meteor.*, **169**, 115–138, doi: 10.1007/s10546-018-0364-4.

Ding, A. J., C. B. Fu, X. Q. Yang, et al., 2013: Ozone and fine particle in the western Yangtze River Delta: An overview of 1 yr data at the SORPES station. *Atmos. Chem. Phys.*, **13**, 5813–5830, doi: 10.5194/acp-13-5813-2013.

Dominici, F., M. Greenstone, and C. R. Sunstein, 2014: Particulate matter matters. *Science*, **344**, 257–259, doi: 10.1126/science.1247348.

Frisch, U., 1995: Turbulence: The legacy of AN Kolmogorov, Cambridge University Press, UK, 72–97.

Gao, S. H., Y. J. Wang, Y. X. Huang, et al., 2016: Spatial statistics of atmospheric particulate matter in China. *Atmos. Environ.*, **134**, 162–167, doi: 10.1016/j.atmosenv.2016.03.052.

Grange, S. K., J. A. Salmond, W. J. Trompetter, et al., 2013: Effect of atmospheric stability on the impact of domestic wood combustion to air quality of a small urban township in winter. *Atmos. Environ.*, **70**, 28–38, doi: 10.1016/j.atmosenv.2012.12.047.

Helgason, W., and J. W. Pomeroy, 2012: Characteristics of the near-surface boundary layer within a mountain valley during winter. *J. Appl. Meteor. Climatol.*, **51**, 583–597, doi: 10.1175/jamc-d-11-058.1.

Hu, J. L., Y. G. Wang, Q. Ying, et al., 2014: Spatial and temporal variability of $PM_{2.5}$ and PM_{10} over the North China Plain and the Yangtze River Delta, China. *Atmos. Environ.*, **95**, 598–609, doi: 10.1016/j.atmosenv.2014.07.019.

Hu, X. M., Y. Zhang, M. Z. Jacobson, et al., 2008: Coupling and evaluating gas/particle mass transfer treatments for aerosol simulation and forecast. *J. Geophys. Res. Atmos.*, **113**, D11208, doi: 10.1029/2007jd009588.

Hu, X. M., P. M. Klein, M. Xue, et al., 2013: Impact of the vertical mixing induced by low-level jets on boundary layer ozone concentration. *Atmos. Environ.*, **70**, 123–130, doi: 10.1016/j.atmosenv.2012.12.046.

Huang, N. E., Z. Shen, S. R. Long, et al., 1998: The empirical mode decomposition and the Hilbert spectrum for nonlinear and non-stationary time series analysis. *Proc. Roy. Soc. A. Math. Phys. Eng. Sci.*, **454**, 903–995, doi: 10.1098/rspa.1998.0193.

Huang, N. E., Z. Shen, and S. R. Long, 1999: A new view of nonlinear water waves: The Hilbert spectrum. *Annu. Rev. Fluid Mech.*, **31**, 417–457, doi: 10.1146/annurev.fluid.31.1.417.

Huang, Y. X., F. G. Schmitt, Z. M. Lu, et al., 2008: An amplitude–frequency study of turbulent scaling intermittency using Empirical Mode Decomposition and Hilbert Spectral Analysis. *EPL (Europhys. Lett.)*, **84**, 40010, doi: 10.1209/0295-5075/84/40010.

Huang, Y. X., F. G. Schmitt, J. P. Hermand, et al., 2011: Arbitrary-order Hilbert spectral analysis for time series possessing scaling statistics: Comparison study with detrended fluctuation analysis and wavelet leaders. *Phys. Rev. E*, **84**, 016208, doi: 10.1103/physreve.84.016208.

Jia, B., Y. Wang, Y. Yao, et al., 2015: A new indicator on the impact of large-scale circulation on wintertime particulate matter pollution over China. *Atmos. Chem. Phys.*, **15**, 11919–11929, doi: 10.5194/acp-15-11919-2015.

Kalthoff, N., V. Horlacher, U. Corsmeier, et al., 2000: Influence of valley winds on transport and dispersion of airborne pollutants in the Freiburg-Schauinsland area. *J. Geophys. Res. Atmos.*, **105**, 1585–1597, doi: 10.1029/1999jd900999.

Karipot, A., M. Y. Leclerc, G. S. Zhang, et al., 2008: Influence of nocturnal low-level jet on turbulence structure and CO_2 flux measurements over a forest canopy. *J. Geophys. Res. Atmos.*, **113**, D10102, doi: 10.1029/2007jd009149.

Klipp, C. L., and L. Mahrt, 2004: Flux-gradient relationship, self-correlation and intermittency in the stable boundary layer. *Quart. J. Roy. Meteor. Soc.*, **130**, 2087–2103, doi: 10.1256/qj.03.161.

Kolmogorov, A. N., 1941: The local structure of turbulence in incompressible viscous fluid for very large Reynolds numbers. *Dokl. Akad. Nauk SRSS*, **30**, 301–305.

Mahrt, L., 1998: Nocturnal boundary-layer regimes. *Bound.-Layer Meteor.*, **88**, 255–278, doi: 10.1023/a:1001171313493.

Mahrt, L., 2014: Stably stratified atmospheric boundary layers. *Annu. Rev. Fluid Mech.*, **46**, 23–45, doi: 10.1146/annurev-fluid-010313-141354.

Miao, Y. C., J. P. Guo, S. H. Liu, et al., 2017: Relay transport of aerosols to Beijing–Tianjin–Hebei region by multi-scale atmospheric circulations. *Atmos. Environ.*, **165**, 35–45, doi: 10.1016/j.atmosenv.2017.06.032.

Miao, Y. C., J. P. Guo, S. H. Liu, et al., 2018: The climatology of low-level jet in Beijing and Guangzhou, China. *J. Geophys. Res. Atmos.*, **123**, 2816–2830, doi: 10.1002/2017jd027321.

Nel, A., 2005: Air pollution-related illness: Effects of particles.

Science, **308**, 804–806, doi: 10.1126/science.1108752.

Noone, D., C. Risi, A. Bailey, et al., 2013: Determining water sources in the boundary layer from tall tower profiles of water vapor and surface water isotope ratios after a snowstorm in Colorado. *Atmos. Chem. Phys.*, **13**, 1607–1623, doi: 10.5194/acp-13-1607-2013.

Petäjä, T., L. Järvi, V. M. Kerminen, et al., 2016: Enhanced air pollution via aerosol-boundary layer feedback in China. *Sci. Rep.*, **6**, 18998, doi: 10.1038/srep18998.

Poulos, G. S., W. Blumen, D. C. Fritts, et al., 2002: CASES-99: A comprehensive investigation of the stable nocturnal boundary layer. *Bull. Amer. Meteor. Soc.*, **83**, 555–581, doi: 10.1175/1520-0477(2002)083<0555:CACIOT>2.3.CO;2.

Quan, J. N., X. X. Tie, Q. Zhang, et al., 2014: Characteristics of heavy aerosol pollution during the 2012–2013 winter in Beijing, China. *Atmos. Environ.*, **88**, 83–89, doi: 10.1016/j.atmosenv.2014.01.058.

Quan, J. N., Q. Liu, X. Li, et al., 2015: Effect of heterogeneous aqueous reactions on the secondary formation of inorganic aerosols during haze events. *Atmos. Environ.*, **122**, 306–312, doi: 10.1016/j.atmosenv.2015.09.068.

Reitebuch, O., A. Strassburger, S. Emeis, et al., 2000: Nocturnal secondary ozone concentration maxima analysed by sodar observations and surface measurements. *Atmos. Environ.*, **34**, 4315–4329, doi: 10.1016/s1352-2310(00)00185-0.

Ren, Y., S. W. Zheng, W. Wei, et al., 2018: Characteristics of turbulent transfer during episodes of heavy haze pollution in Beijing in winter 2016/17. *J. Meteor. Res.*, **32**, 69–80, doi: 10.1007/s13351-018-7072-3.

Rodriguez, A., A. Sánchez-Arcilla, J. M. Redondo, et al., 1995: Pollutant dispersion in the nearshore region: Modelling and measurements. *Water Sci. Technol.*, **32**, 169–178, doi: 10.1016/0273-1223(96)00088-1.

Salmond, J. A., 2005: Wavelet analysis of intermittent turbulence in a very stable nocturnal boundary layer: Implications for the vertical mixing of ozone. *Bound.-Layer Meteor.*, **114**, 463–488, doi: 10.1007/s10546-004-2422-3.

Salmond, J. A., and I. G. McKendry, 2005: A review of turbulence in the very stable nocturnal boundary layer and its implications for air quality. *Prog. Phys. Geogr.: Earth Environ.*, **29**, 171–188, doi: 10.1191/0309133305pp442ra.

Schäfer, K., S. Emeis, H. Hoffmann, et al., 2006: Influence of mixing layer height upon air pollution in urban and sub-urban areas. *Meteor. Z.*, **15**, 647–658, doi: 10.1127/0941-2948/2006/0164.

Seibert, P., H. Feldmann, B. Neininger, et al., 2000: South foehn and ozone in the eastern Alps—Case study and climatological aspects. *Atmos. Environ.*, **34**, 1379–1394, doi: 10.1016/s1352-2310(99)00439-2.

Shao, P. Y., H. Z. Tian, Y. J. Sun, et al., 2018: Characterizing remarkable changes of severe haze events and chemical compositions in multi-size airborne particles (PM_1, $PM_{2.5}$ and PM_{10}) from January 2013 to 2016–2017 winter in Beijing, China. *Atmos. Environ.*, **189**, 133–144, doi: 10.1016/j.atmosenv.2018.06.038.

Shen, Z., G. X. Cui, and Z. S. Zhang, 2017: Turbulent dispersion of pollutants in urban-type canopies under stable stratification conditions. *Atmos. Environ.*, **156**, 1–14, doi: 10.1016/j.atmosenv.2017.02.017.

Sorbjan, Z., and A. Czerwinska, 2013: Statistics of turbulence in the stable boundary layer affected by gravity waves. *Bound.-Layer Meteor.*, **148**, 73–91, doi: 10.1007/s10546-013-9809-y.

Strassburger, A., and W. Kuttler, 1998: Diurnal courses of ozone in an inner urban park. *Meteor. Z.*, **7**, 15–18, doi: 10.1127/metz/7/1998/15.

Tang, G., X. Li, Y. Wang, et al., 2009: Surface ozone trend details and interpretations in Beijing, 2001–2006. *Atmos. Chem. Phys.*, **9**, 8813–8823, doi: 10.5194/acp-9-8813-2009.

Tang, G. Q., J. Q. Zhang, X. W. Zhu, et al., 2016: Mixing layer height and its implications for air pollution over Beijing, China. *Atmos. Chem. Phys.*, **16**, 2459–2475, doi: 10.5194/acp-16-2459-2016.

Tao, S., Y. Wang, S. M. Wu, et al., 2007: Vertical distribution of polycyclic aromatic hydrocarbons in atmospheric boundary layer of Beijing in winter. *Atmos. Environ.*, **41**, 9594–9602, doi: 10.1016/j.atmosenv.2007.08.026.

Terradellas, E., M. R. Soler, E. Ferreres, et al., 2005: Analysis of oscillations in the stable atmospheric boundary layer using wavelet methods. *Bound.-Layer Meteor.*, **114**, 489–518, doi: 10.1007/s10546-004-1293-y.

Thompson, T. M., R. K. Saari, and N. E. Selin, 2014: Air quality resolution for health impact assessment: Influence of regional characteristics. *Atmos. Chem. Phys.*, **14**, 969–978, doi: 10.5194/acp-14-969-2014.

Vindel, J. M., and C. Yagüe, 2011: Intermittency of turbulence in the atmospheric boundary layer: Scaling exponents and stratification influence. *Bound.-Layer Meteor.*, **140**, 73–85, doi: 10.1007/s10546-011-9597-1.

Walters, J. T., R. T. McNider, X. Z. Shi, et al., 2007: Positive surface temperature feedback in the stable nocturnal boundary layer. *Geophys. Res. Lett.*, **34**, L12709, doi: 10.1029/2007gl029505.

Wang, G., S. Y. Cheng, J. B. Li, et al., 2015: Source apportionment and seasonal variation of $PM_{2.5}$ carbonaceous aerosol in the Beijing–Tianjin–Hebei region of China. *Environ. Monit. Assess.*, **187**, 143, doi: 10.1007/s10661-015-4288-x.

Wang, H., J. X. Xu, M. Zhang, et al., 2014: A study of the meteorological causes of a prolonged and severe haze episode in January 2013 over central–eastern China. *Atmos. Environ.*, **98**, 146–157, doi: 10.1016/j.atmosenv.2014.08.053.

Wang, L. L., N. Zhang, Z. R. Liu, et al., 2014: The influence of climate factors, meteorological conditions, and boundary-layer structure on severe haze pollution in the Beijing–Tianjin–Hebei region during January 2013. *Adv. Meteor.*, 685971, doi: 10.1155/2014/685971.

Wang, T., W. Nie, J. Gao, et al., 2010: Air quality during the 2008 Beijing Olympics: Secondary pollutants and regional impact. *Atmos. Chem. Phys.*, **10**, 7603–7615, doi: 10.5194/acp-10-7603-2010.

Wang, X. F., W. X. Wang, L. X. Yang, et al., 2012: The secondary formation of inorganic aerosols in the droplet mode through heterogeneous aqueous reactions under haze conditions. *Atmos. Environ.*, **63**, 68–76, doi: 10.1016/j.atmosenv.2012.09.029.

Wang, Y., M. B. McElroy, J. W. Munger, et al., 2008: Variations of O_3 and CO in summertime at a rural site near Beijing. *Atmos. Chem. Phys.*, **8**, 6355–6363, doi: 10.5194/acp-8-6355-2008.

Wang, Z. F., J. Li, Z. Wang, et al., 2014: Modeling study of regional severe hazes over mid-eastern China in January 2013 and its implications on pollution prevention and control. *Sci. China Earth Sci.*, **57**, 3–13, doi: 10.1007/s11430-013-4793-0.

Wei, W., F. G. Schmitt, Y. X. Huang, et al., 2016: The analyses of turbulence characteristics in the atmospheric surface layer using arbitrary-order Hilbert spectra. *Bound.-Layer Meteor.*, **159**, 391–406, doi: 10.1007/s10546-015-0122-9.

Wei, W., H. S. Zhang, F, G. Schmitt, et al., 2017: Investigation of turbulence behaviour in the stable boundary layer using arbitrary-order Hilbert spectra. *Bound.-Layer Meteor.*, **163**, 311–326, doi: 10.1007/s10546-016-0227-9.

Wei, W., M. Z. Wang, H. S. Zhang, et al., 2019: Diurnal characteristics of turbulent intermittency in the Taklimakan Desert. *Meteor. Atmos. Phys.*, **131**, 287–297, doi: 10.1007/s00703-017-0572-3.

Xia, H. X., 2006: The preliminary study of introducing the superhigh chimney to the plain area of Beijing. *Municipal Administration & Technology*, **8**, 70–72, doi: 10.3969/j.issn.1008-2271.2006.02.009. (in Chinese)

Yagüe, C., S. Viana, G. Maqueda, et al., 2006: Influence of stability on the flux-profile relationships for wind speed, Φ_m, and temperature, Φ_h, for the stable atmospheric boundary layer. *Nonlinear Process. Geophys.*, **13**, 185–203, doi: 10.5194/npg-13-185-2006.

Ye, X. X., Y. Song, X. H. Cai, et al., 2016: Study on the synoptic flow patterns and boundary layer process of the severe haze events over the North China Plain in January 2013. *Atmos. Environ.*, **124**, 129–145, doi: 10.1016/j.atmosenv.2015.06.011.

Yin, Z. C., and H. J. Wang, 2017: Role of atmospheric circulations in haze pollution in December 2016. *Atmos. Chem. Phys.*, **17**, 11673–11681, doi: 10.5194/acp-17-11673-2017.

Yu, L. D., G. F. Wang, R. J. Zhang, et al., 2013: Characterization and source apportionment of $PM_{2.5}$ in an urban environment in Beijing. *Aerosol Air Qual. Res.*, **13**, 574–583, doi: 10.4209/aaqr.2012.07.0192.

Zhang, H. F., S. X. Wang, J. M. Hao, et al., 2016: Air pollution and control action in Beijing. *J. Clean. Prod.*, **112**, 1519–1527, doi: 10.1016/j.jclepro.2015.04.092.

Zhang, J. P., T. Zhu, Q. H. Zhang, et al., 2012: The impact of circulation patterns on regional transport pathways and air quality over Beijing and its surroundings. *Atmos. Chem. Phys.*, **12**, 5031–5053, doi: 10.5194/acp-12-5031-2012.

Zheng, G. J., F. K. Duan, H. Su, et al., 2015: Exploring the severe winter haze in Beijing: The impact of synoptic weather, regional transport and heterogeneous reactions. *Atmos. Chem. Phys.*, **15**, 2969–2983, doi: 10.5194/acp-15-2969-2015.

Zheng, S., A. Pozzer, C. X. Cao, et al., 2015: Long-term (2001–2012) concentrations of fine particulate matter ($PM_{2.5}$) and the impact on human health in Beijing, China. *Atmos. Chem. Phys.*, **15**, 5715–5725, doi: 10.5194/acp-15-5715-2015.

Zhong, J. T., X. Y. Zhang, Y. Q. Wang, et al., 2017: Relative contributions of boundary-layer meteorological factors to the explosive growth of $PM_{2.5}$ during the red-alert heavy pollution episodes in Beijing in December 2016. *J. Meteor. Res.*, **31**, 809–819, doi: 10.1007/s13351-017-7088-0.

Tech & Copy Editor: Zhirong CHEN